Electronic Supplementary Material (ESI) for Journal of Materials Chemistry A.

Rational Design of Bifunctional ORR/OER Catalysts Based on Pt/Pd-Doped Nb_2CT_2 MXene by First-Principles Calculations

Dongxiao Kan [a], Dashuai Wang [a], Xilin Zhang [b], Ruqian Lian [a], Jing Xu [a,c], Gang Chen [a], and Yingjin Wei [a] *

[a] Key Laboratory of Physics and Technology for Advanced Batteries (Ministry of Education), Jilin Engineering Laboratory of New Energy Materials and Technology, College of Physics, Jilin University, Changchun 130012, P.R. China.

[b] College of Physics and Materials Science, Henan Normal University, Xinxiang, Henan 453007, P.R. China.

[c] Department of Physics, College of Science, Yanbian University, Yanji 133002, P.R. China.

[*] Corresponding author

Email: yjwei@jlu.edu.cn (Y. J. Wei)

Tel: 86-431-85155126

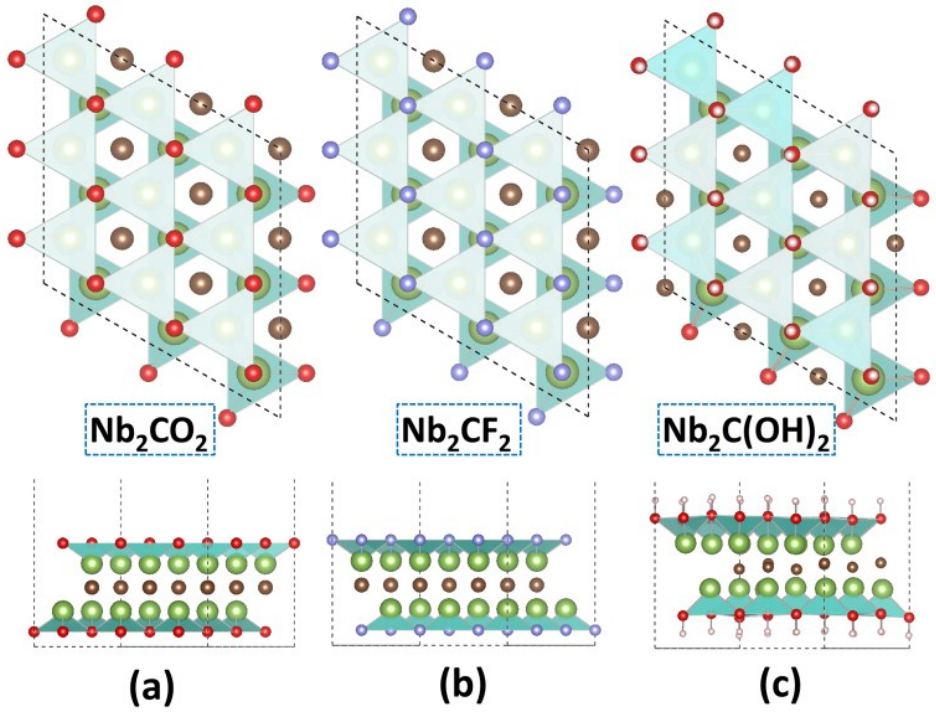

Figure S1 The structures of terminated Nb_2C, **a)** Nb_2CO_2, **b)** Nb_2CF_2, and **c)** $Nb_2C(OH)_2$.

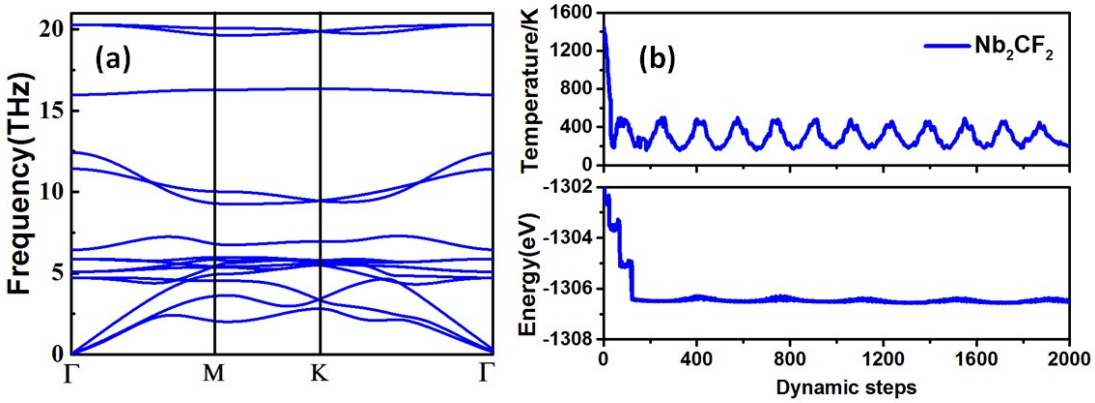

Figure S2 a) The Frequency distribution of geometrically optimized Nb_2CF_2, **b)** Temperature equilibrium curve and energy fluctuation curve obtained from molecule dynamic simulation.

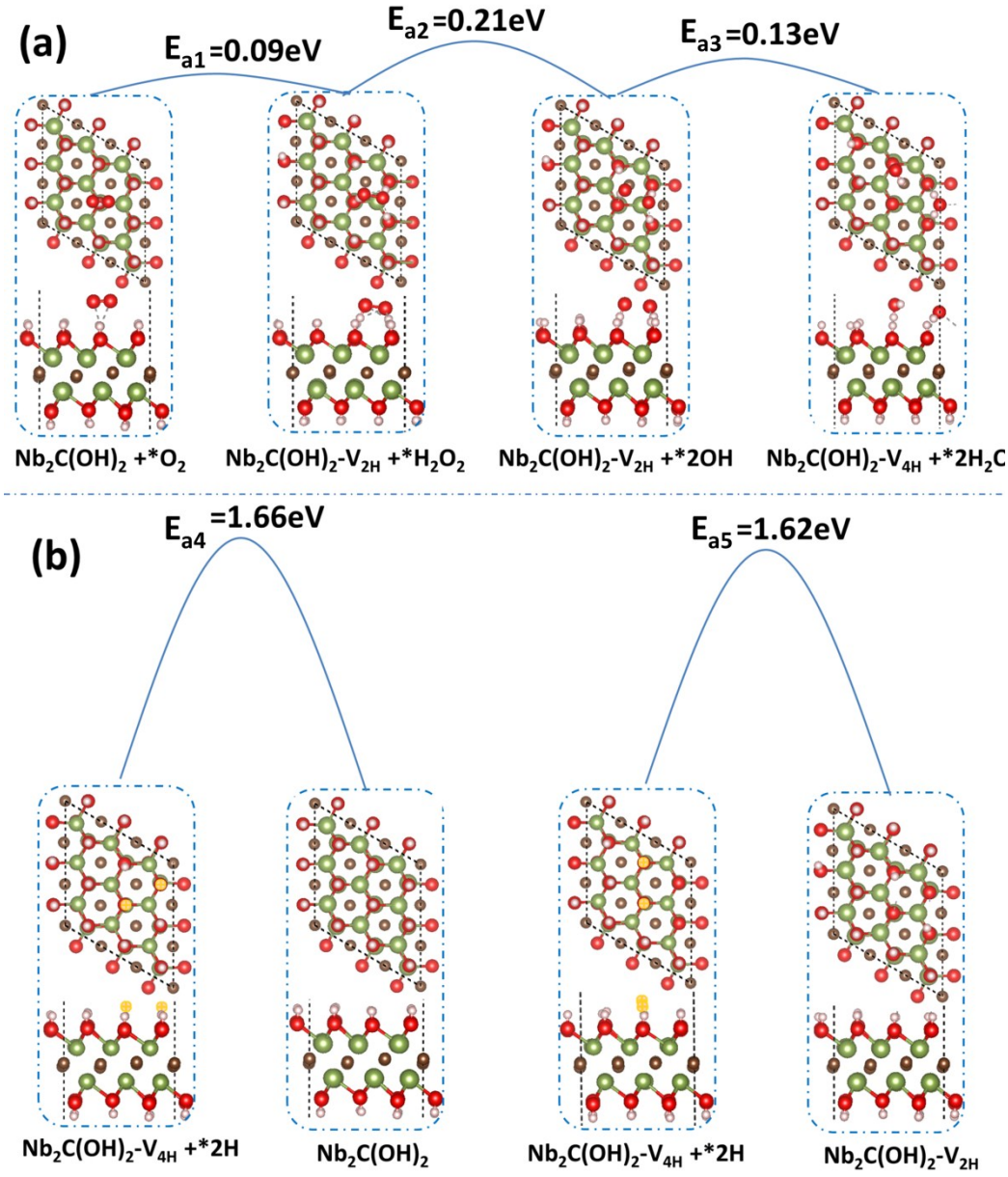

Figure S3 The reaction paths and the activation barriers of **a)** ORR on $Nb_2C(OH)_2$ and **b)** OH groups recovery.

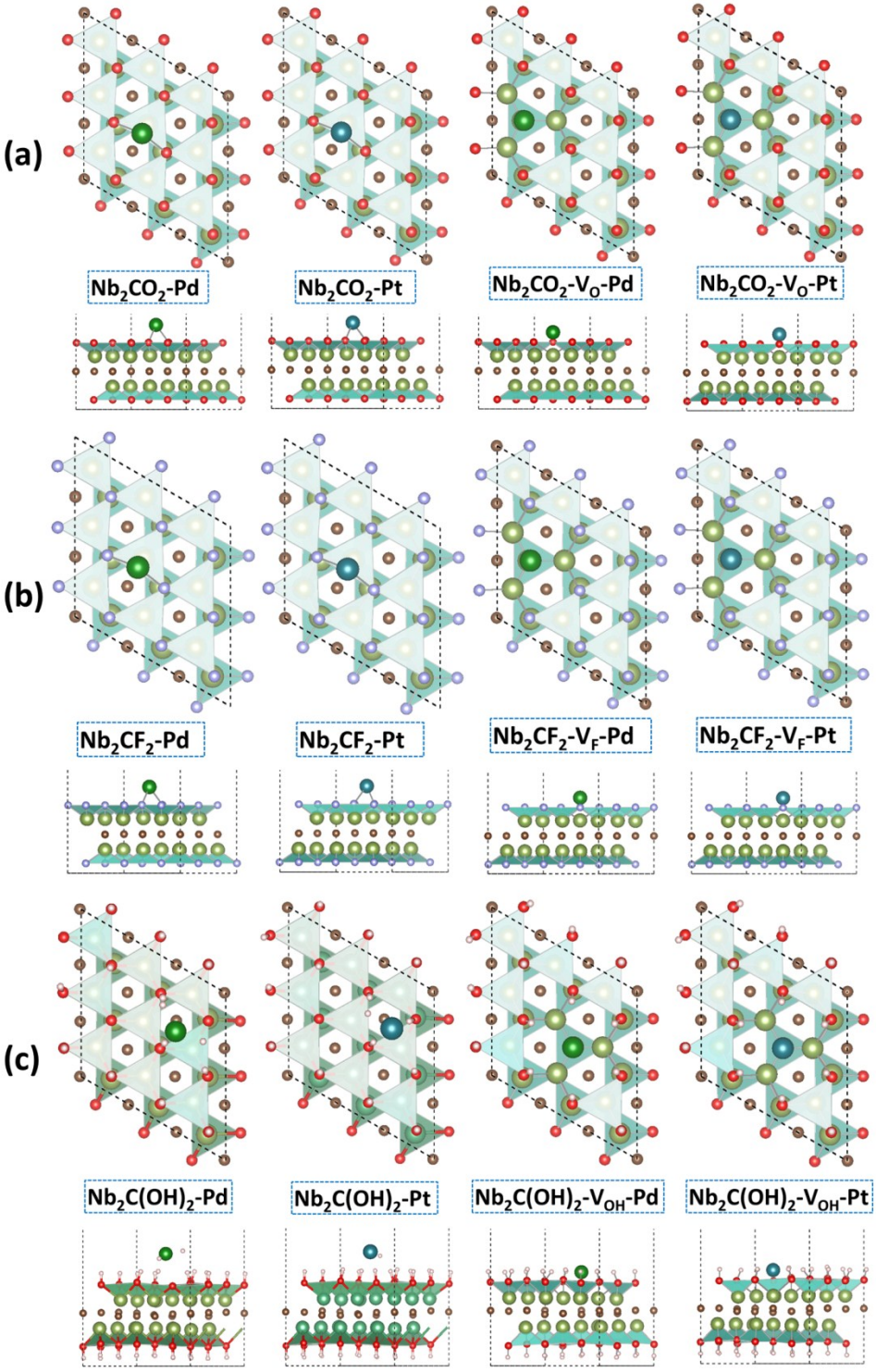

Figure S4 The structures of the recombinant catalysts, with **a)** Pt/Pd single atoms on O-terminated Nb_2C, **b)** Pt/Pd single atoms on F-terminated Nb_2C, and **c)** Pt/Pd single atoms on OH-terminated Nb_2C.

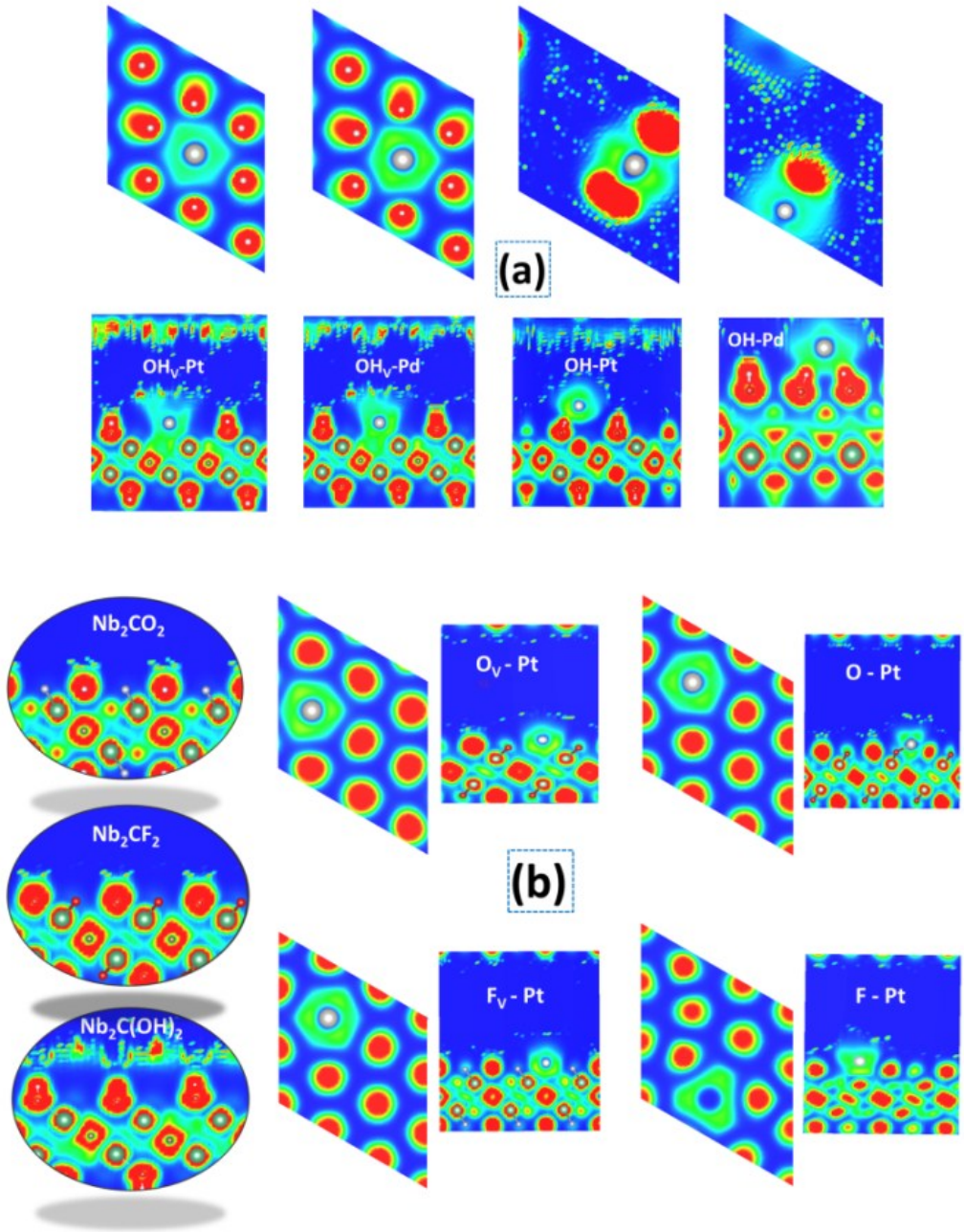

Figure S5 The electronic locational functions (ELF) of **a)** Pt/Pd single atoms on $Nb_2C(OH)_2$ and **b)** functional terminated Nb_2C and Pt/Pd single atoms on Nb_2CO_2 and Nb_2CF_2.

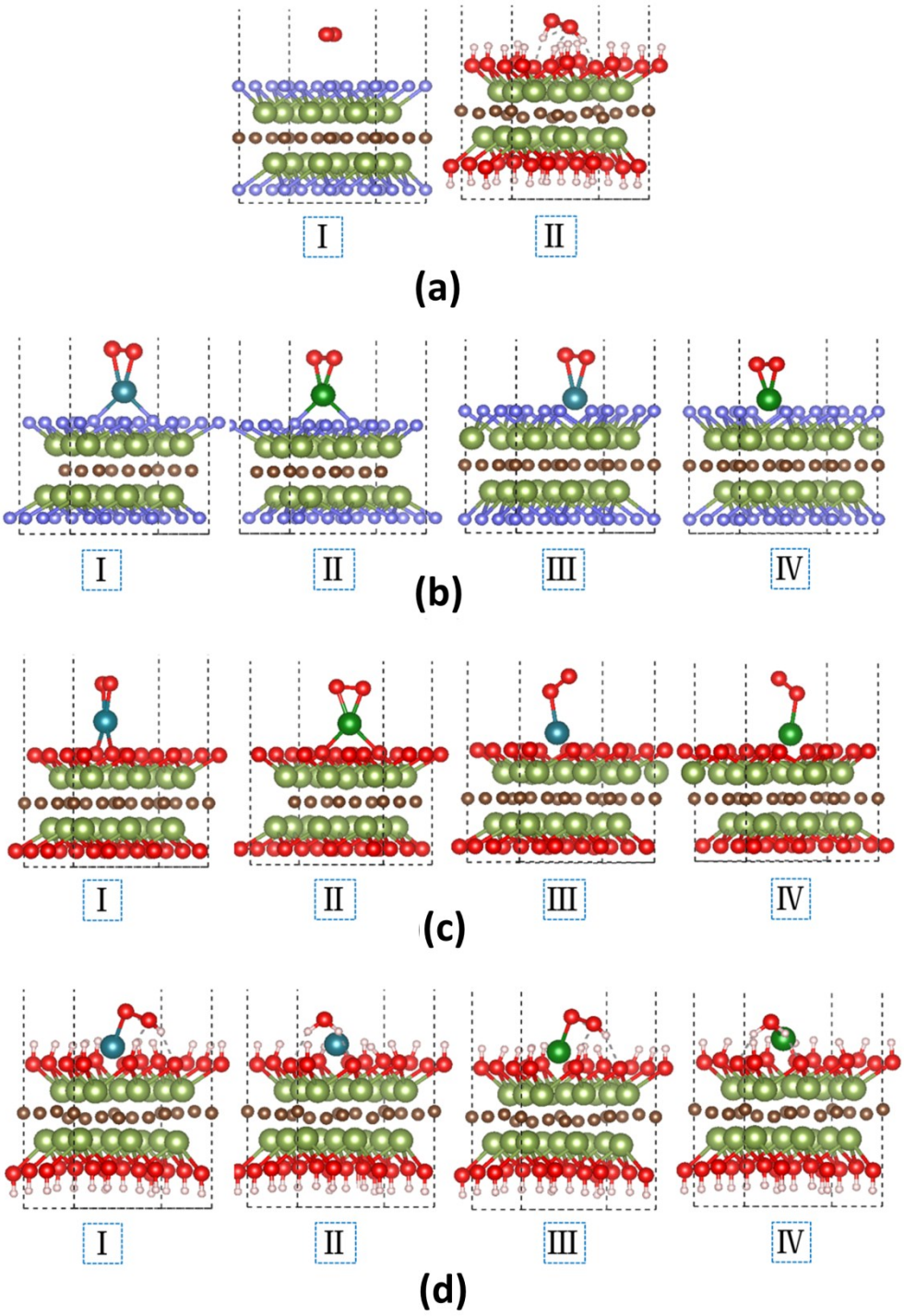

Figure S6 The adsorption properties of O_2 molecules on **a)** Nb_2CF_2, $Nb_2C(OH)_2$ and **b)-d)** Pt/Pd single atoms modified Nb_2CF_2, Nb_2CO_2 and $Nb_2C(OH)_2$, respectively.

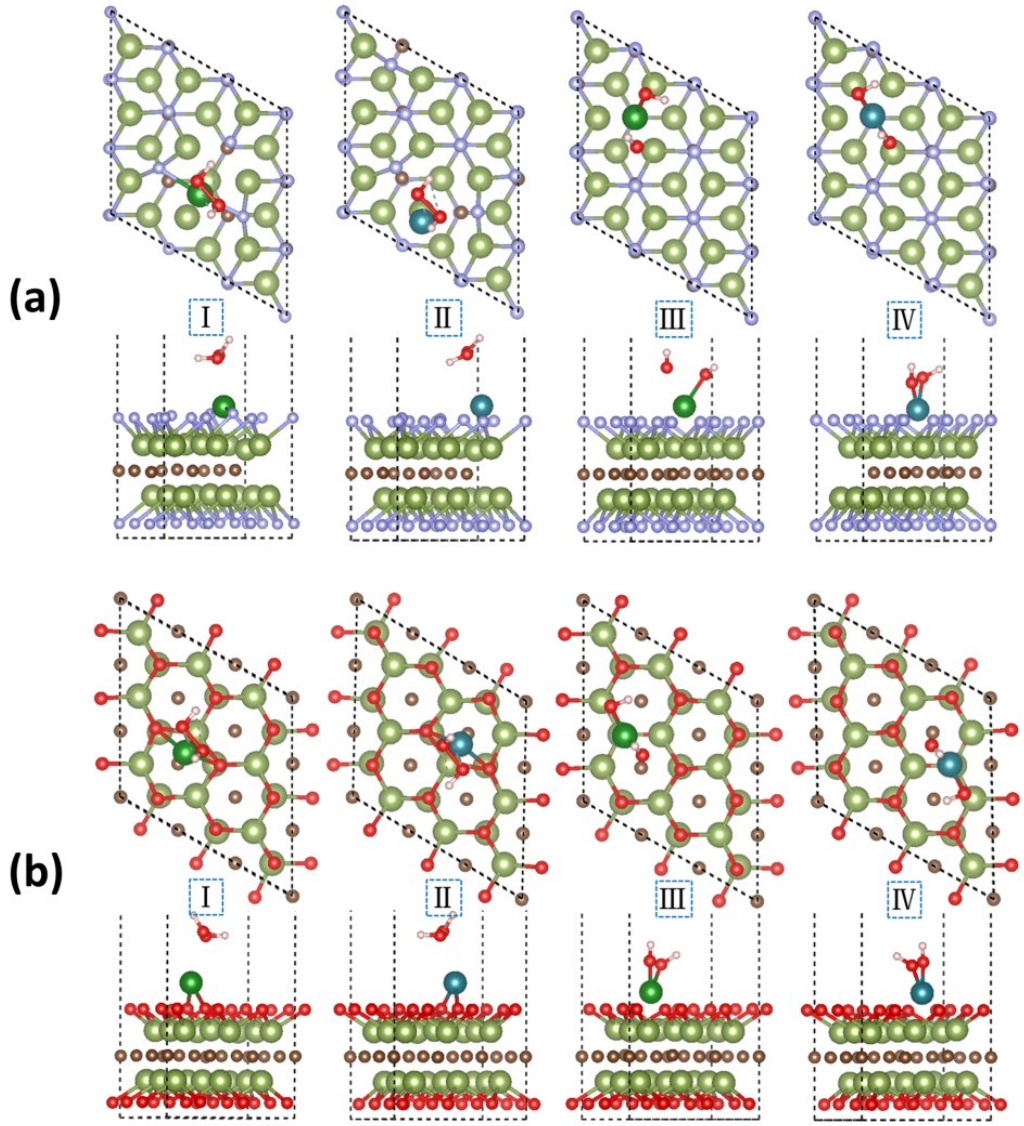

Figure S7 The adsorption properties of H_2O_2 molecules on **a)** Pt/Pd single atoms modified Nb_2CF_2, and **b)** Pt/Pd single atoms modified Nb_2CO_2.

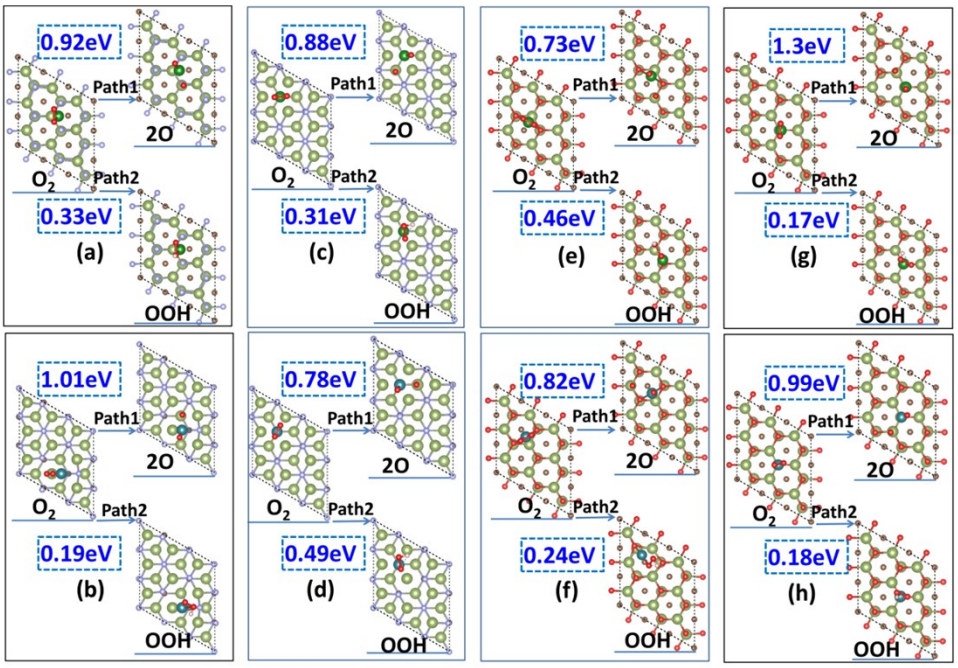

Figure S8 The reaction competition of O_2 hydrogenation (path 2) or dissociation (path1) at the first step of ORR**, a)-h)** represented Nb_2CO_2-Pd, Nb_2CO_2-Pt, Nb_2CF_2-Pd, Nb_2CF_2-Pt, Nb_2CO_2-V_O-Pd, Nb_2CO_2-V_O-Pt, Nb_2CF_2-V_F-Pd, Nb_2CF_2-V_F–Pt, respectively.

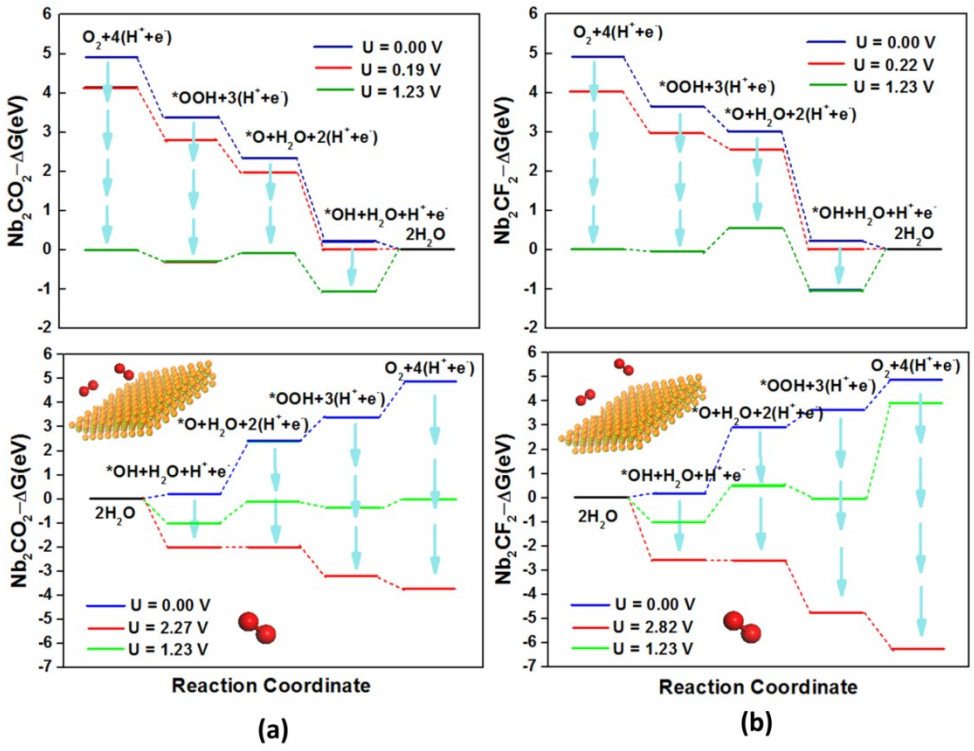

Figure S9 Changes in Gibbs free energy differences (ΔG) of elementary reaction steps along the 4-*e*- pathway toward ORR and OER, with **a)** ΔG for Nb_2CO_2, and **b)** ΔG for Nb_2CF_2, respectively.

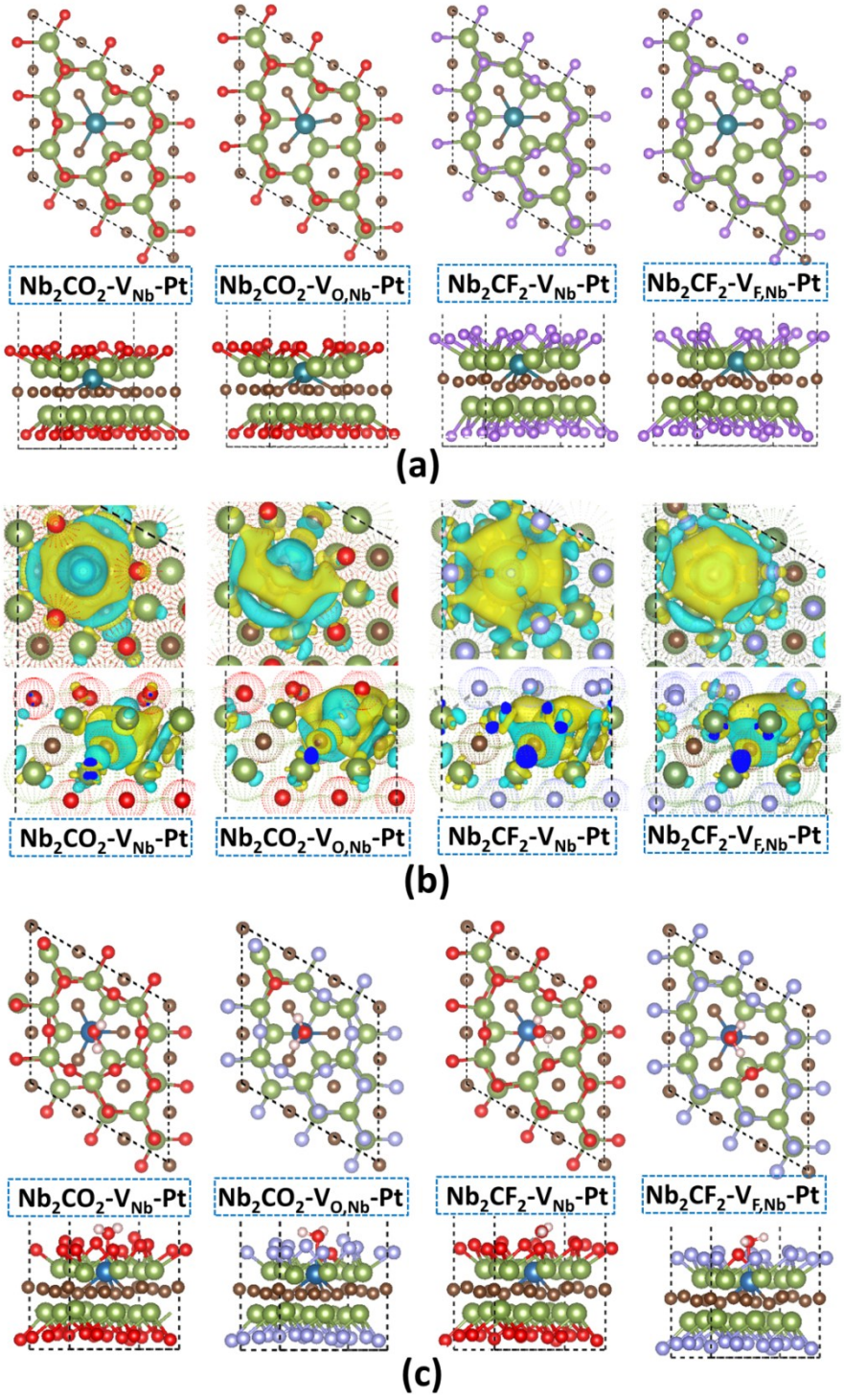

Figure S10 a) The structure of Nb-deficit vacancies immobilized with single Pt atoms; **b)** the charge transfer differences (CDD) of the structures of Nb_2CO_2-V_{Nb}-Pt , Nb_2CF_2-V_{Nb}-Pt, Nb_2CO_2-$V_{Nb,O}$-Pt and Nb_2CF_2-$V_{Nb,F}$-Pt; **c)** H_2O_2 molecule adsorbed on the Nb-deficit structures with or without the functional vacancies.

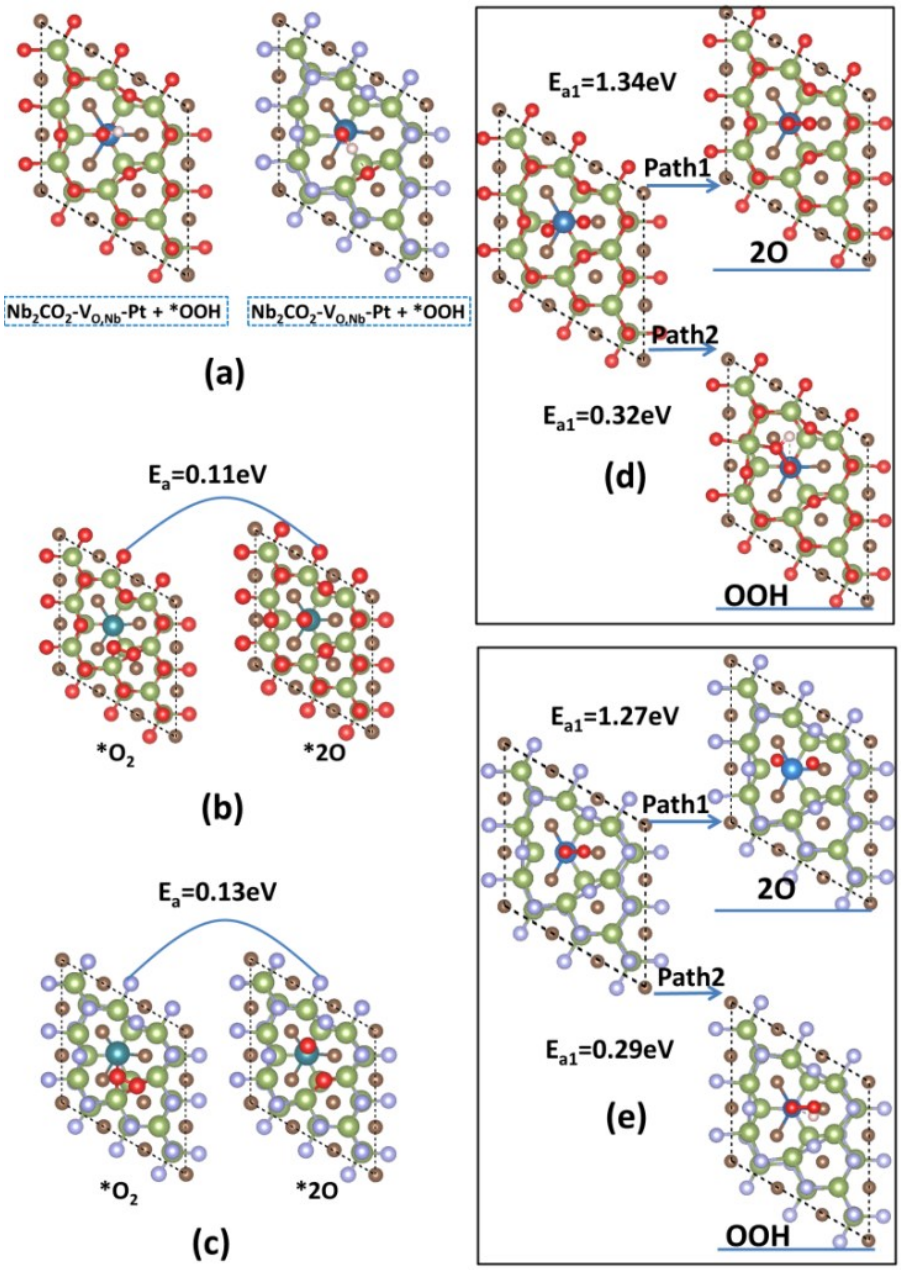

Figure S11 a) The adsorption properties of OOH on the Nb-defected MXenes; **b)-c)** the reaction paths and barrier of O_2 dissociation on Nb_2CO_2-V_{Nb} -Pt and Nb_2CF_2-V_{Nb}-Pt; **d)-e)** the reaction competition in the first step of ORR on Nb_2CO_2-$V_{Nb,O}$-Pt and Nb_2CF_2-$V_{Nb,F}$-Pt, respectively.

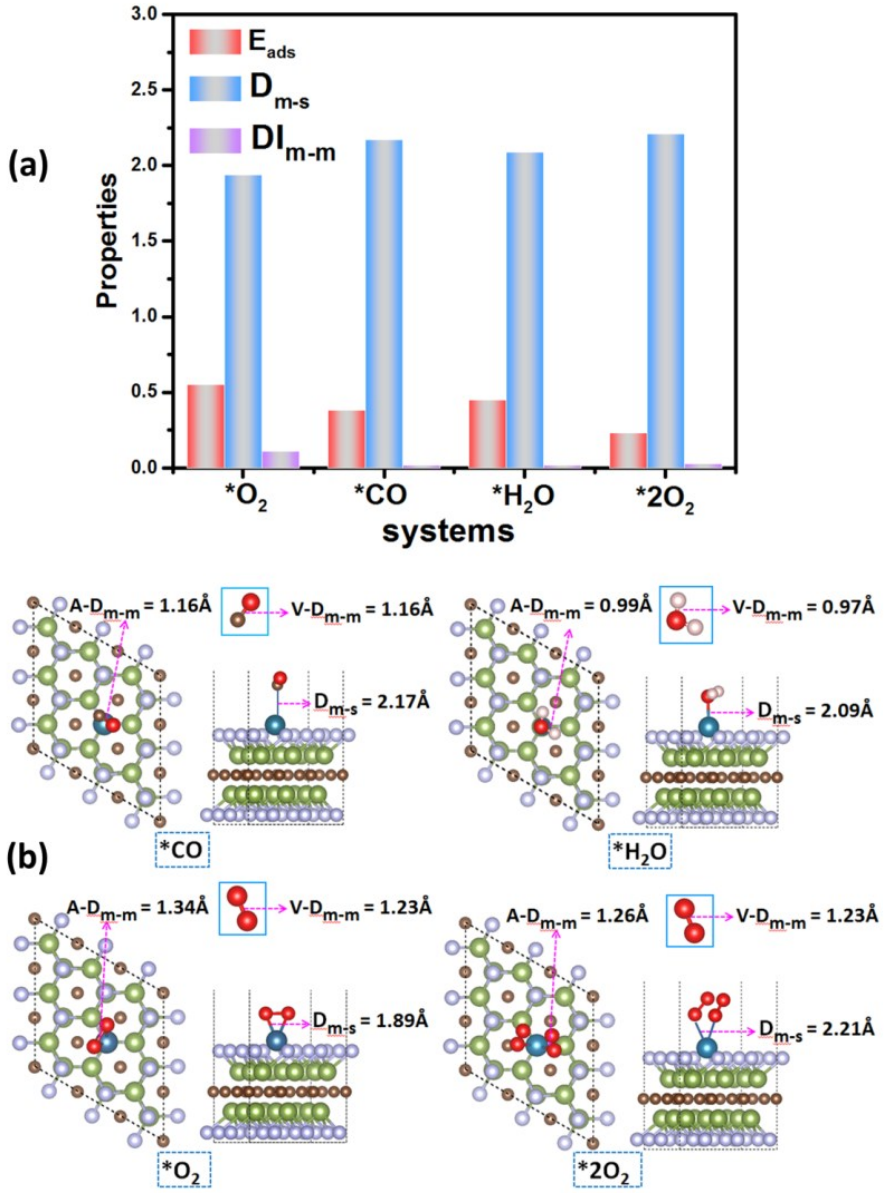

Figure S12 The properties **a)** and structures **b)** of molecules (O_2, CO, H_2O and double O_2) adsorbed on Nb_2CF_2-V_F-Pt, where D_{m-s} represented the distance between the adsorbents and substrate, D_{m-m} and DI_{m-m} were the bond lengthes of molecules in vacuum and increased bond lengthes of the activated molecules, respectively.

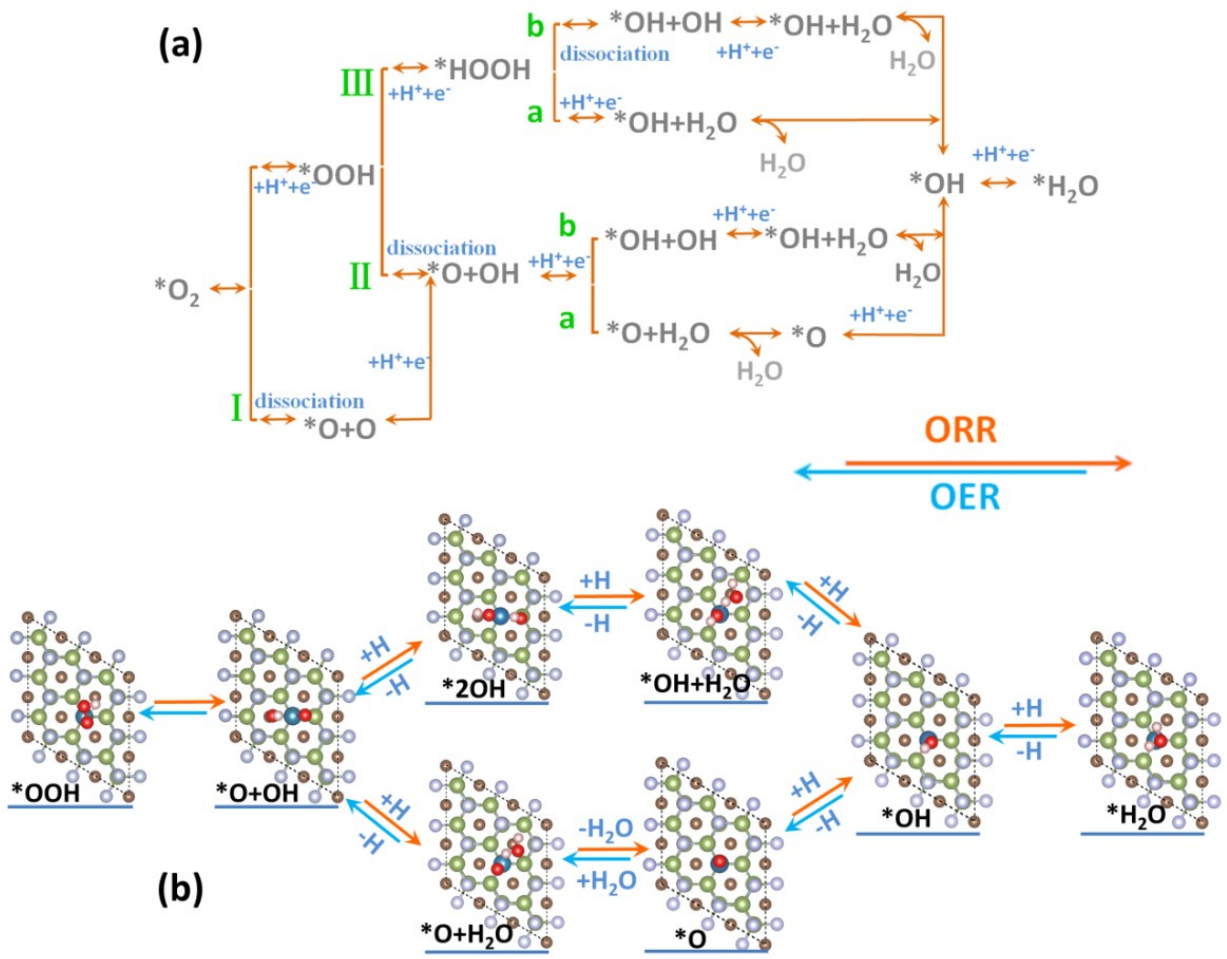

Figure S13 a) Schematic diagram of possible reaction pathways for ORR. **b)** The possible reaction pathways for the ORR on Nb_2CF_2-V_F-Pt.

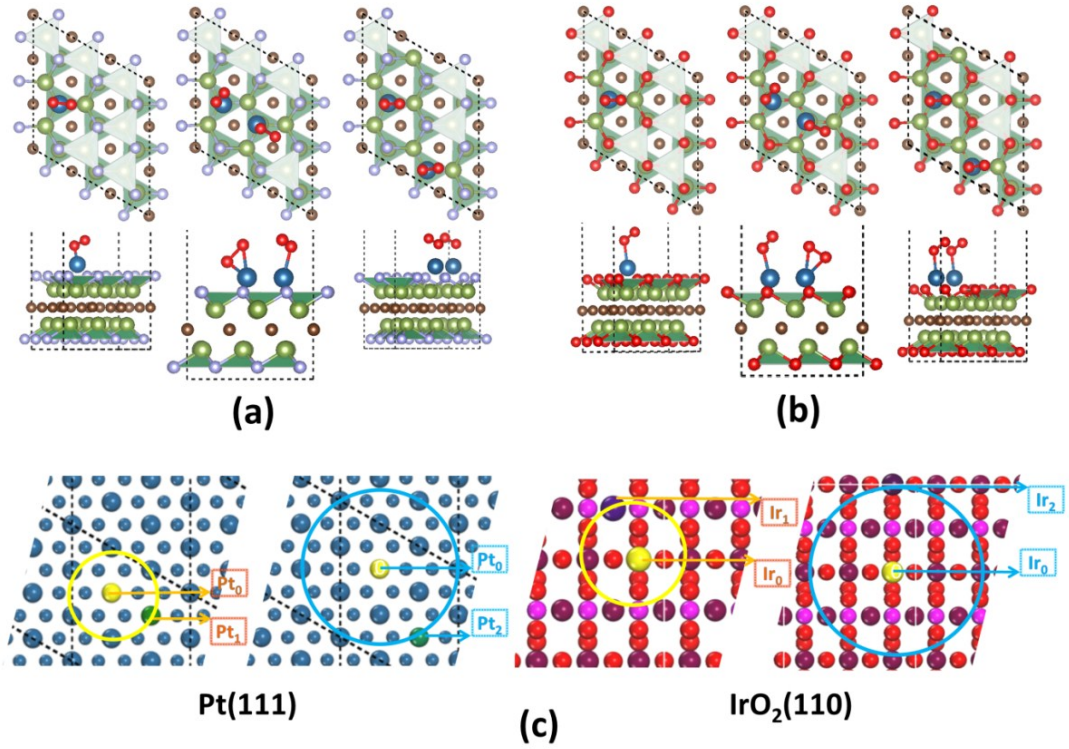

Figure S14 The adsorption structures of O_2 on **a)** Nb_2CO_2-V_O-Pt, Nb_2CO_2-V_O-Pt_0Pt_1, Nb_2CO_2-V_O-Pt_0Pt_2 and **b)** Nb_2CF_2-V_F-Pt Nb_2CF_2-V_F-Pt_0Pt_1, Nb_2CF_2-V_F-Pt_0Pt_2. **c)-d)** the scheme of noble metal utilization on Pt(111) and IrO_2(110), respectively.

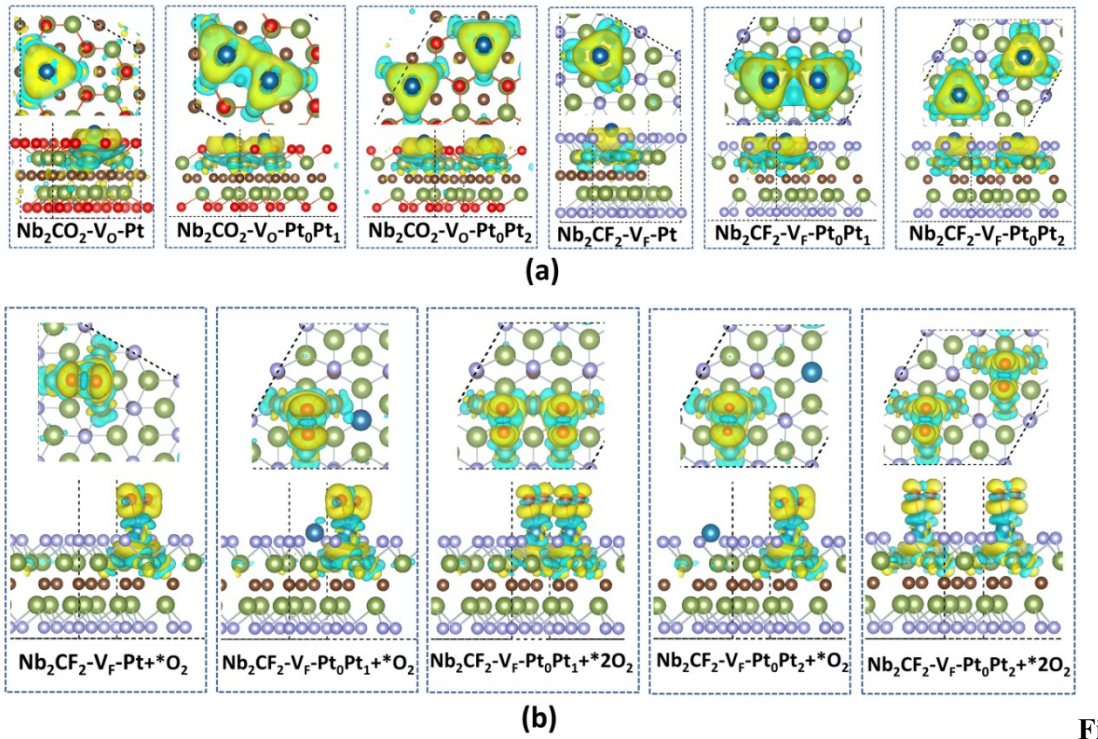

Fi

gure S15 a) The charge density differences (CDD) of Nb_2CO_2-V_O-Pt_0Pt_1, Nb_2CO_2-V_O-Pt_0Pt_2, Nb_2CF_2-V_F-Pt_0Pt_1, and Nb_2CF_2-V_F-Pt_0Pt_2. **b)** The CDD of a single or a double O_2 adsorbed Nb_2CF_2-V_F-Pt_0Pt_1 and Nb_2CF_2-V_F-Pt_0Pt_2.

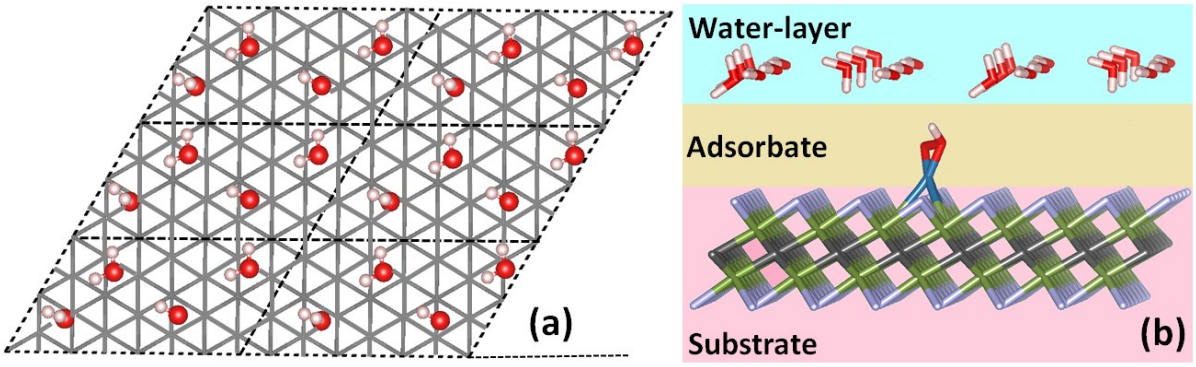

Figure S16 a) The top view of the solvation system and b) the solvation model with adsorbed intermediates.

Table S1. The adsorption properties of the reaction molecule O_2 on Nb_2CT_X, in which E_{ads}-O_2 was the adsorption energies and Q was the number of charge transfer from catalysts to O_2. And η^{ORR} and η^{ORR} were the overpotentials toward ORR and OER.

Properties	**E_{ads}-O_2(eV)**	**η^{ORR}(V)**	**η^{OER}(V)**	**Q(e)**
Nb_2C	**-11.47**	**---**	**---**	**1.23**
Nb_2CO_2	**-0.29**	**1.04**	**0.94**	**0.17**
Nb_2CF_2	**-0.22**	**1.04**	**1.53**	**0.21**
$Nb_2C(OH)_2$	**-0.92**	**---**	**---**	**0.88**

Table S2. The adsorption energy of a O_2 molecular on different catalysts, where E_{ads}-0, E_{ads}-1 and E_{ads}-2 represented the adsorption energies of O_2 on noble metals which was labeled as Pt_0, Pt_1, Pt_2 and Ir_0, Ir_1, Ir_2 respectively.

Properties	**E_{ads}-0(eV）**	**E_{ads}-1(eV）**	**E_{ads}-2(eV）**
Nb_2CO_2-V_O-Pt_0Pt_1	**0.50**	**0.41**	
Nb_2CO_2-V_O-Pt_0Pt_2	**0.65**		**0.65**
Nb_2CF_2-V_F-Pt_0Pt_1	**0.46**	**0.38**	
Nb_2CF_2-V_F-Pt_0Pt_2	**0.56**		**0.56**
Pt(111)-Pt_0Pt_1	**-0.53**	**-0.39**	
Pt(111)-Pt_0Pt_2	**-0.69**		**-0.69**
IrO2(110)-Ir_0Ir_1	**-0.18**	**-0.14**	
IrO2(110)-Ir_0Ir_2	**-0.22**		**-0.22**

Table S3. Charge transfer during the reactions, Q-0, Q-1, Q-2 were the charge number that noble metals gained from the supports, Q_1-O_2 and Q_2-O_2 were the charge number of the first and second O_2 molecule captured from catalysts.

Properties	**Q-0(e)**	**Q-1(e)**	**Q-2(e)**	**Q_1-O_2(e)**	**Q_2-O_2(e)**
Nb_2CO_2-V_O-Pt_0Pt_1	**0.47**	**0.42**	**---**	**0.48**	**0.45**
Nb_2CO_2-V_O-Pt_0Pt_2	**0.51**	**---**	**0.51**	**0.57**	**0.57**
Nb_2CF_2-V_F-Pt_0Pt_1	**0.40**	**0.36**	**---**	**0.42**	**0.41**
Nb_2CF_2-V_F-Pt_0Pt_2	**0.48**	**---**	**0.48**	**0.53**	**0.53**

Table S4 The energy corrections and the adsorption free energies in ORR and OER on all the catalysts.

	ΔZPE	TΔS	ΔG	ΔZPE	TΔS	ΔG
	Nb_2CO_2			Nb_2CF_2		
*OOH	0.51	0.26	3.35	0.51	0.27	3.65
*O	0.10	0.13	2.36	0.10	0.13	3.02
*OH	0.40	0.13	0.19	0.39	0.13	0.22
	Nb_2CO_2-Pd			Nb_2CF_2-Pd		
*OOH	0.50	0.24	4.59	0.51	0.28	4.47
*O	0.10	0.13	3.24	0.10	0.13	2.79
*OH	0.40	0.13	1.79	0.41	0.12	1.37
	Nb_2CO_2-Pt			Nb_2CF_2-Pt		
*OOH	0.51	0.26	3.75	0.50	0.26	3.92
*O	0.10	0.13	2.85	0.10	0.09	2.27
*OH	0.40	0.12	0.51	0.39	0.13	0.52
	Nb_2CO_2-V_O-Pd			Nb_2CF_2-V_F-Pd		
*OOH	0.52	0.26	4.20	0.49	0.26	4.16
*O	0.11	0.13	2.51	0.10	0.10	3.04
*OH	0.40	0.13	1.14	0.40	0.13	0.93
	Nb_2CO_2-V_O-Pt			Nb_2CF_2-V_F-Pt		
*OOH	0.52	0.27	3.81	0.51	0.28	3.85
*O	0.11	0.10	2.38	0.10	0.13	2.25
*OH	0.40	0.13	0.76	0.39	0.14	0.83

Table S5 The solvation energies corrections (ΔSol) and the free energies after considering the salvation effect (ΔG_{Sol}) on the selected catalysts (Nb_2CO_2-V_O-Pt and Nb_2CF_2-V_F-Pt).

	ΔSol			**ΔG_{Sol}**		
	***OOH**	***O**	***OH**	***OOH**	***O**	***OH**
Nb_2CO_2-V_O-Pt	**-0.57**	**-0.50**	**-0.62**	**4.18**	**2.31**	**0.88**
Nb_2CF_2-V_F-Pt	**-0.45**	**-0.59**	**-0.56**	**4.02**	**2.39**	**0.80**

The poison resistance of Nb_2CF_2-V_F-Pt

To evaluate the poison resistance of Nb_2CF_2-V_F-Pt, we studied the adsorption properties of CO, H_2O and multiple O_2 on the selected catalyst. As shown in Figure S12a, the E_{ads} represented the adsorption energies of several molecules on Nb_2CF_2-V_F-Pt. It revealed that the catalyst had the strongest binding strength to O_2 molecules, with the largest E_{ads} (0.55 eV). Then followed by the H_2O molecule (0.49 ev), which indicated that O_2 was adsorbed first in the reaction. As to the CO and the second O_2, the adsorption energies were only 0.38 and 0.23 eV, respectively, which manifested that Nb_2CF_2-V_F-Pt had the resistance to CO poisoning, moreover multiple O_2 wouldn't prevent the subsequent reactions. Besides, the distance between the adsorbents and substrate (D_{m-s}) was shortest and the increased bond length of the activated molecules (DI_{m-m}) was the longest on the adsorbed O_2 (Figure S12). It indicated that the O_2 were activated to the greatest extent among these adsorbates, which further demonstrated that Nb_2CF_2-V_F-Pt will not be poisoned during the catalytic process.

The reaction energies barriers of ORR/OER on Nb_2CF_2-V_F-Pt

Although there were three possible reaction pathways (I-III) in the schematic diagram (Figure S13a), association mechanism of ORR was more feasible on Nb_2CF_2-V_F-Pt (II) (Figure S13b), where the adsorbed O_2 molecule went through a sequential coupled proton-electron transfer process to form H_2O through the following reactions:

$$* + O_2 + H^+ + e^- \rightarrow *OOH \text{ (R1-II)}$$

$$*OOH \rightarrow O* + OH* \text{ (R2-II)}$$

$$*OOH + H^+ + e^- \rightarrow *O + H_2O \text{ (R2-IIa)}$$

$$OOH* + H+ + e- \rightarrow 2*OH \text{ (R2-IIb)}$$

$$*O + H^+ + e^- \rightarrow *OH \text{ (R3-IIb)}$$

$$2*OH+ H^+ + e^- \rightarrow *OH+ H_2O \text{ (R3-IIa)}$$

$$*OH + H^+ + e^- \rightarrow H_2O \text{ (R4-II)}$$

After the *OOH was formed, it dissociated to *O and *OH with an activation barrier of 0.50 eV. This was followed by two possible reaction paths. One was the OH* hydrogenation to

release a H_2O molecule (R4-IIa) firstly and then the remained *O was reduced to *OH and H_2O (R5-IIa) with activation barriers of 0.71, 0.62 and 0.73 eV, respectively. The other path was the *O reduced to form *OH and H_2O with activation barriers of 0.69 and 0.75 eV. In addition, the OER on Nb_2CF_2-V_F-Pt is followed by a reversed process of ORR, in which the absorbed H_2O species directly dissociated to *OH and dissociative H atom in the first step with an energy barrier of 0.67eV. Then the produced *OH met with two reaction bench. In path IIa, the *OH further dissociated to *O and H atom, then the remained *O captured a H_2O and dissociated to *O and *OH with an activation barrier of 0.75 and 0.70 eV, respectively. While in path IIb, *OH combined with a H_2O molecule to form 2*OH and then dehydrogenated to *O and *OH with an energy barrier of 0.88 and 1.03 eV, respectively. Therewith, the produced *O and *OH synthesized to the *OOH and finally separated out O_2 with energy barriers of 0.67 and 53eV, respectively.

The Solvation effect

Based on previous studies, a single ice-like bilayer of water is a reasonable model able to provide sufficient water molecules to describe solvation effects.[1] To fit the size of water bilayer, the repeating unit of Nb_2CO_2-V_O-Pt and Nb_2CF_2-V_F-Pt was increased from 3×3 to 7×5, and the water layer was constructed in a 2×3 repeating unit including 24 H_2O molecules (Figure S16). The energy correction of the solvation energy (ΔSol) was defined by the following equations (equation 1-2):

$$\Delta Sol = E_{tot} - E_{(sur\ +\ adsorbate)} - E_{water} + E_{(sur\ +\ water)} \quad (1)$$

$$\Delta G = \Delta E + \Delta ZPE - T\Delta S + \Delta Sol + xeU - 4eU \quad (2)$$

where E_{tot}, $E_{(sur + adsorbate)}$, E_{water}, and $E_{(sur + water)}$ represent the computed electronic energies of the surface with the adsorbates as well as the single water layer, the surface with the adsorbates only, the single water layer, and the surface with single water layer only, respectively. The number of transferred electrons x was 1-3 for the OOH*, O*, and OH* intermediates, respectively.

Results in Table S5 indicated that the intermediates involved in ORR and OER were stabilized to different extents by interacting with environmental water molecules via hydrogen

bonds. As shown, OH* had larger solvation energy compared to OOH* due to its ability to form a more polarized structure on the Nb_2CO_2-V_O-Pt and Nb_2CF_2-V_F-Pt surface. The adsorption of these intermediates was able to keep the binding network in the water bilayer via formation of hydrogen bonds with the neighboring *H_2O molecules. The hydrogen bonds interaction between water bilayer and the intermediates had a certain influence on the whole ORR process of Nb_2CO_2-V_O-Pt and Nb_2CF_2-V_F-Pt, and the overpotentials were changed (0.49V and 0.43 V). Besides, the rate-limiting steps of OER were turned to *O+H_2O →*OOH + H^+ + e^- both on Nb_2CO_2-V_O-Pt and Nb_2CF_2-V_F-Pt. Accompanying with this, the OER overpotentials shifted from 0.39 to 0.64 V (Nb_2CO_2-V_O-Pt) and from 0.37 to 0.40 V (Nb_2CF_2-V_F-Pt). The above results indicated that, although water indeed influenced the absolute adsorption energy and free energy of the reactions, it didn't significantly affect the general trend of the inherent catalytic properties.

More calculation details

The overall ORR reaction in the acidic environment was written in Eq (3), like that occurs on the cathode of a fuel cell in discharge:

$$O_2 + 4H^+ + 4e^- \rightarrow 2H_2O \quad (3)$$

According to literatures, this ORR reaction proceeded via the 4-electron transfer pathways as shown in Eq 3a-3d:

$$* + O_2\ (g) + e^- + H^+ \rightarrow {}^*OOH \quad (3a)$$

$${}^*OOH + e^- + H^+ \rightarrow H_2O\ (l) + {}^*O \quad (3b)$$

$$O^* + e^- + H^+ \rightarrow {}^*OH \quad (3c)$$

$${}^*OH + e^- + H^+ \rightarrow H_2O\ (l) + * \quad (3d)$$

In which * denoted an activity site on the catalyst, (l) and (g) represented liquid and gas phases, respectively. The adsorption energies of O-containing intermediates on the catalysts were

calculated by Eq (4)-(7):

$$\Delta E_{O*} = E_{O*} - E_{*} - [E_{H_2O} - E_{H_2}] \quad (4)$$

$$\Delta E_{OH*} = E_{OH*} - E_{*} - [E_{H_2O} - 1/2E_{H_2}] \quad (5)$$

$$\Delta E_{OOH*} = E_{OOH*} - E_{*} - [2E_{H_2O} - 3/2E_{H_2}] \quad (6)$$

Where E_*, E_{OOH*}, E_{OH*}, and E_{O*} referred to the total energies of the catalyst substrate without and with the adsorption of OOH, OH and O, respectively. And E_{H2O} and E_{H2} were the total energies of free H_2O and H_2 molecules in gas phases, respectively. For each step, the reaction Gibbs free energy ΔG was defined by the Eq (7)

$$\Delta G = \Delta E + \Delta ZPE - T\Delta S + \Delta G_U + \Delta G_{pH} \quad (7)$$

Here, ΔZPE was the zero-point energy which could be obtained from the calculation of vibrational frequencies for the adsorbed species. ΔS was the entropy of the reaction. In fact, the ΔZPE and the entropy of the adsorbed O-containing intermediates on different catalysts were found to have similar values (Table S4).

The OER was the reverse reaction of ORR that described in Eq (8):

$$2H_2O \rightarrow O_2 + 4e^- + 4H^+ \quad (8)$$

with the 4-electron transfer pathways given in Eq 8a-8d:

$$H_2O\ (l) + * \rightarrow {}^*OH + e^- + H^+ \quad (8a)$$

$${}^*OH \rightarrow O^* + e^- + H^+ \quad (8b)$$

$$H_2O\ (l) + {}^*O \rightarrow {}^*OOH + e^- + H^+ \quad (8c)$$

$${}^*OOH \rightarrow * + O_2\ (g) + e^- + H^+ \quad (8d)$$

The computational ΔG for each step was used to determine the rate-determining step during the reactions. The theoretical maximum free energy change for ORR (ΔG_{max}^{123}) and OER ($\Delta G_{max}^{123'}$) at equilibrium potential was obtained by

$$\Delta G_{max}^{123} = \max \{\Delta G_a, \Delta G_b, \Delta G_c, \Delta G_d\} + 1.23V \quad (9)$$

$$\Delta G_{max}^{123'} = \max \{-\Delta G_{a'}, -\Delta G_{b'}, -\Delta G_{c'}, -\Delta G_{d'}\} + 1.23V \quad (10)$$

References

1. J. A. Gauthier, C. F. Dickens, L. D. Chen, A. D. Doyle and J. K. Nørskov, *The Journal of Physical Chemistry C*, 2017, **121**, 11455-11463.